

Article

Contributions of Microbial “Contact Leaching” to Pyrite Oxidation under Different Controlled Redox Potentials

Bingxu Dong^{1,2,3}, Yan Jia^{1,2}, Qiaoyi Tan^{1,2,4}, Heyun Sun^{1,2} and Renman Ruan^{1,2,4,*}

¹ CAS Key Laboratory of Green Process and Engineering, Institute of Process Engineering, Chinese Academy of Sciences, Beijing 100190, China; bxdong@ipe.ac.cn (B.D.); yjia@ipe.ac.cn (Y.J.); qytan@ipe.ac.cn (Q.T.); sunhy@ipe.ac.cn (H.S.)

² National Engineering Laboratory for Hydrometallurgical Cleaner Production Technology, Chinese Academy of Sciences, Beijing 100190, China

³ University of Chinese Academy of Sciences, Beijing 100049, China

⁴ State Key Laboratory of Biochemical Engineering Institute of Process Engineering, Chinese Academy of Sciences, Beijing 100190, China

* Correspondence: rmruan@ipe.ac.cn

Received: 1 September 2020; Accepted: 21 September 2020; Published: 29 September 2020



Abstract: The function of microbial contact leaching to pyrite oxidation was investigated by analyzing the differences of residue morphologies, leaching rates, surface products, and microbial consortia under different conditions in this study. This was achieved by novel equipment that can control the redox potential of the solution and isolate pyrite from microbial contact oxidation. The morphology of residues showed that the corruptions were a little bit severer in the presence of attached microbes under 750 mV and 850 mV (vs. SHE). At 650 mV, the oxidation of pyrite was undetectable even in the presence of attached microbes. The pyrite dissolution rate was higher with attached microbes than that without attached microbes at 750 mV and 850 mV. The elemental sulfur on the surface of pyrite residues with sessile microorganisms was much less than that without attached microbes at 750 mV and 850 mV, showing that sessile acidophiles may accelerate pyrite leaching by reducing the elemental sulfur inhibition. Many more sulfur-oxidizers were found in the sessile microbial consortium which also supported the idea. The results suggest that the microbial “contact leaching” to pyrite oxidation is limited and relies on the elimination of elemental sulfur passivation by attached sulfur-oxidizing microbes rather than the contact oxidation by EPS-Fe.

Keywords: pyrite bioleaching; contact leaching; controlled redox potential; elemental sulfur inhibition; microbial consortium

1. Introduction

Pyrite (FeS_2) is the most abundant sulfide mineral on the earth. The oxidation of pyrite is an indispensable part of a global circulation of iron and sulfur [1]. Pyrite always intergrows with Cu, Co, and Zn and serves as the most prevalent host of gold. Therefore, pyrite bioleaching is useful for the extraction of a variety of useful metals [2]. Bioleaching is also used in treating spent catalysts to recover a lot of valuable metal [3,4]. When exposed to the atmosphere, pyrite generates an acidic, metal-enriched effluent, so-called “acid mine drainage” (AMD), which is accelerated by the growth of microbes and is harmful to the environment [5]. Consequently, investigating the pyrite leaching mechanisms and microbes’ functions are both vital for mining and environmental protection.

The mechanism of pyrite oxidation has been proposed as a thiosulfate mechanism, in which the bonds between iron and sulfur moiety can only be broken by the attack of ferric ions. Thiosulfate

is believed to be the first free sulfur compound in the oxidation process [6]. Then the ferrous iron was oxidized into ferric iron and thiosulfate was oxidized into sulfate through a series of reactions. Pyrite oxidation is known as an electrochemical process [7]. The redox potential of solution is critically correlated with the pyrite dissolution rate. Sun et al. [8] found the leaching rate increased by five-fold when redox potential was increased by 100 mV. The pyrite leaching rate is also affected by the oxidizing agent, particle size, and temperature [9]. However, pyrite is inert when the solution has low redox potential [10,11] and the oxidation can be detected only at the redox potential above 660 mV [12]. The redox potential mainly depends on the activities of ferrous ions and ferric ions under bioleaching conditions, which means the pyrite would leach quicker when there is a higher percentage of ferric ions in the solution. Pyrite is oxidized via thiosulfate [13,14]. Most thiosulfate is degraded into sulfate and some elemental sulfur is formed as a side product in a cyclic process [15].

The mechanism of pyrite bioleaching has attracted researchers for a long time. Silverman and Ehrlich first proposed the bioleaching mechanisms as a “direct mechanism” and “indirect mechanism” [16]. No enzymatic interaction between cells and minerals was found, so the “contact leaching” was put forward [17]. Sand et al. [15] further developed the “indirect mechanism” into a “non-contact mechanism” and “contact mechanism”, which has been widely accepted now. The “non-contact mechanism” can be explained as follows: the microorganisms oxidize the dissolved ferrous ions into ferric ions, which can attack metal sulfides. The existence of “non-contact mechanisms” has already been proved. In a “contact mechanism”, microbial cells are attached to the surface of the sulfide, and the extracellular polymeric substance (EPS) complexed ferric ions can mediate the sulfide mineral oxidation and cell attachment [18]. However, this process is not completely confirmed because it is difficult to completely exclude the effect of the “non-contact mechanism”. For example, some researchers claimed that the cell-sized pits in the ore surface implied the function of a “contact mechanism”. However pure chemical oxidation can cause cell-size pits as well [8,19]. So, when investigating the “contact mechanism” about pyrite, it is important to control the effect of “non-contact leaching”. In bioleaching, a large number of microbial cells attach to the mineral surface, while a small proportion of cells are planktonic in solution, as revealed in recent research [20]. Chemotaxis response and wetting behavior of the substrates can affect the microbial adsorption significantly. Pre-colonized species can affect latter attachment, and cell attachment performance is varied even between mixed cultures and pure cultures alone [21,22]. The function of the attached microbes is very critical to study.

Acidophilic microorganisms, including iron-, sulfur-oxidizing bacteria, and archaea, accelerate the oxidation of pyrite by mediating the production of ferric iron and sulfate [23]. The most extensively studied iron-oxidizing microorganisms are *Acidithiobacillus* spp. and *Leptospirillum* spp. that can catalyze the oxidation of ferrous iron to increase the redox potential of the solution and have a primary role in accelerating pyrite bio-oxidation. As the most widely studied Archaea, *Ferroplasma* spp., oxidizes ferrous and can survive in a much harsher environment [24]. Sulfur oxidizers usually oxidize the reduced sulfur and produce sulfate acid. As a typical sulfur oxidizer, *Acidithiobacillus caldus* cannot oxidize the pyrite directly, but can accelerate pyrite leaching in mixed cultures [25]. However, the studies seldom directly confirm the function of microbes to pyrite leaching under controlled solution Eh. What is more, the microbial consortia vary between sessile and planktonic microorganisms [26]. Therefore, the study about how different species play different roles in pyrite oxidation is meaningful.

In this work, the redox potentials of the reaction solution were controlled by an electric current and a harmless reagent. The morphology of residue and leaching rate showed the contribution of attached microbes. The functions of attached microorganisms to pyrite bioleaching under different redox potentials were studied by investigating the surface product and the microbial consortium composition on residue samples.

2. Materials and Methods

2.1. Apparatus

The reaction system used in this work is shown in Figure 1. The system mainly consists of four parts: redox potential control unit, leaching unit, microbe cultivating unit, and solution circulation system. The redox potential control unit can use the electric current and peroxide solution to control the redox potential of the solution. The electrolysis cell is made of polytetrafluoroethylene (PTFE) and is connected to the solution circulation system. The volume of the electrolysis cell is 100 mL. Both cathode and anode (4.5 cm² of surface area, respectively) are made of platinum. The current of 0.1 A is supplied to the electrolysis cell by a DC power system. The redox potential of the solution in leaching unit is measured by a platinum ring electrode with a combined Ag/AgCl reference electrode (3 M KCl). All potentials have been converted to the standard hydrogen electrode (SHE). The signal collected by the electrode is analyzed by the ORP controller, which would control the DC power system to reduce ferric ions if the redox potential of solution exceeds the setting value. When the redox potential of solution is below the setting value, a 15% peroxide solution is titrated into the electrolysis cell by a peristaltic pump controlled by the ORP controller. The fluctuation of the redox potential of the solution is within ± 5 mV of the setting value.

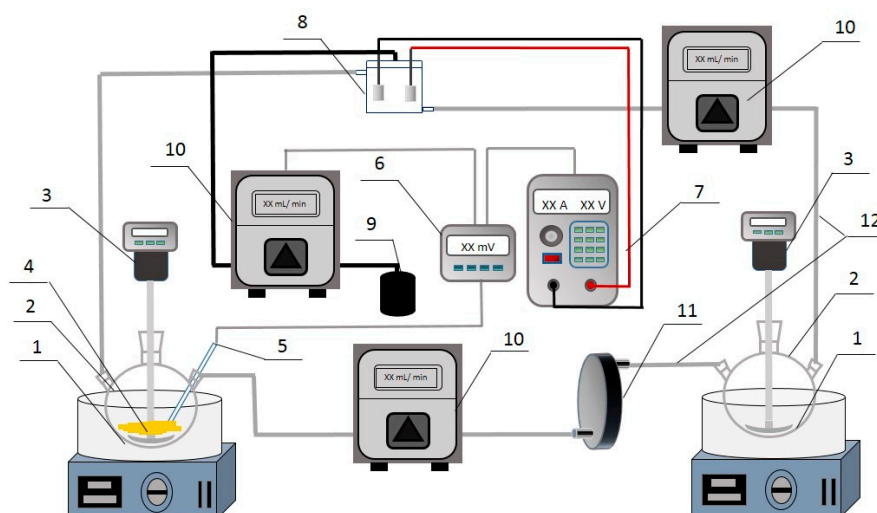


Figure 1. Apparatus for pyrite leaching under controlled redox potentials. (1—constant temperature bath; 2—round-bottom flask; 3—over head stirrer; 4—pyrite sample; 5—ORP probe; 6—ORP controller; 7—DC power system; 8—electrolysis cell; 9—H₂O₂ solution; 10—peristaltic pump; 11—filter plate; 12—silicone tube).

A filter plate is installed between the leaching unit and the microbe cultivating unit. Pyrite samples and half of the medium were added to the leaching unit and bacteria and the left medium were added to the microbe cultivating unit in the beginning. In “non-contact leaching experiments”, a 0.22- μ m micro-porous membrane is installed in the filter plate, which can prevent microorganisms from attaching to pyrite, so only ferric attack or called “non-contact mechanism” can work. In “contact leaching” experiments, no membrane is installed in the filter plate, so microbes can circulate with solution, which means microbes can attach to pyrite. Therefore, both the “non-contact mechanism” and “contact mechanism” can work on pyrite leaching. The solution circulation system connects the two flasks, electrolysis cell, and filter plate together by silicone tubes. The solution cyclically flows pushing by two peristaltic pumps at a speed of 20 mL·min⁻¹ and all ions are distributed uniformly.

2.2. Pyrite Samples

Highly pure pyrite from the Banlao mine (origin Yunnan province, China) was used. The crystalline phase of pyrite was analyzed using powder X-ray diffraction (XRD) (Smartlab (9), Rigaku, Japan), and the data were analyzed by HighScore Plus with PDF4+ database (Figure 2). The results of inductively coupled plasma optical emission spectrometry (ICP-OES) (Optima 5300DV, PerkinElmer, Waltham, MA, USA) showed that the atomic ratio of S to Fe was 2.01, and the total impurity content was less than 0.3%. The pyrite was first crushed into mm-size grains with a hammer, then grinded with an agate mortar and pestle, and finally the samples were wet sieved to obtain 75 to 106 μm particles. The samples were treated with a 50 $^{\circ}\text{C}$ hydrochloric acid solution ($3\text{ mol}\cdot\text{L}^{-1}$) for 30 min and ultrasonically washed in alcohol twice [27,28]. Pyrite residue was vacuum-filtered and dried in a vacuum oven. For SEM measurements, pyrite was cut into rectangular slabs approximately $10\text{ mm} \times 10\text{ mm} \times 3\text{ mm}$, then grinded and polished. At last, they were treated by hydrochloric acid and alcohol like the pyrite power sample.

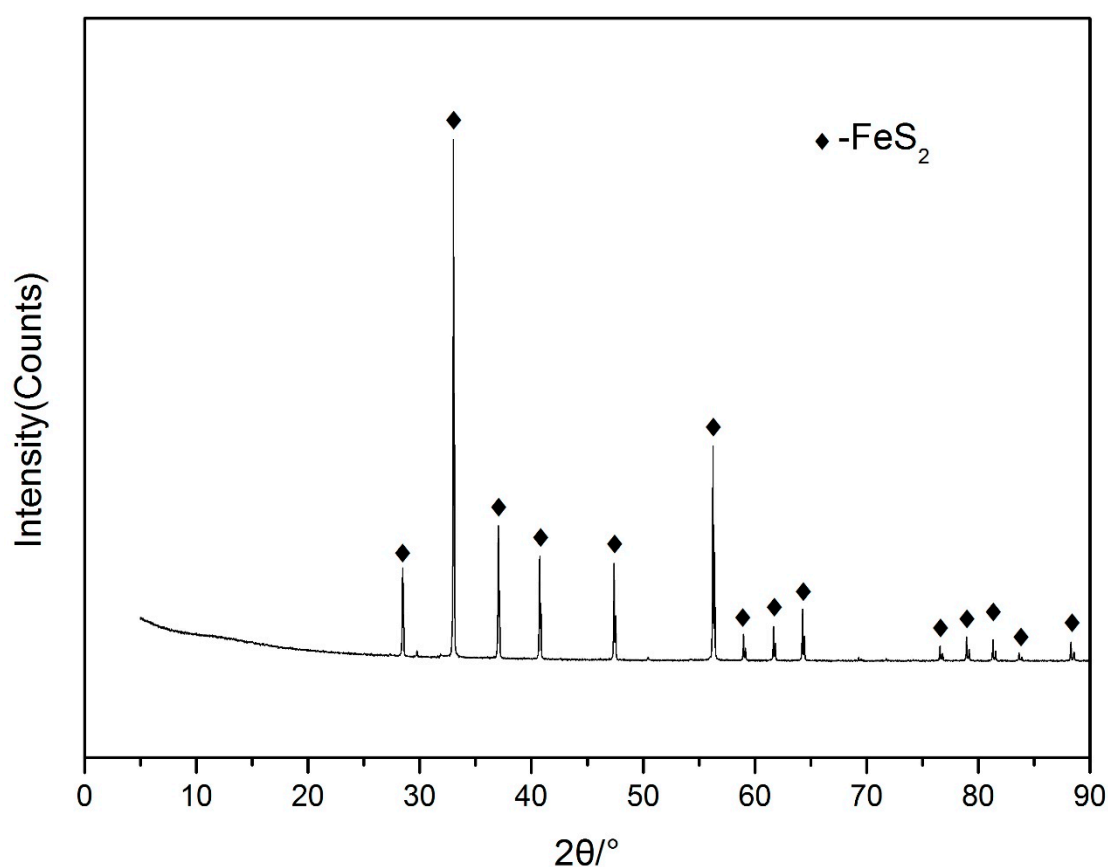


Figure 2. XRD spectra of pyrite sample.

2.3. Culture Medium

Modified 9K solution was used in the experiments [29]: $(\text{NH}_4)_2\text{SO}_4$ $3\text{ g}\cdot\text{L}^{-1}$, KCl $0.1\text{ g}\cdot\text{L}^{-1}$, K_2HPO_4 $0.5\text{ g}\cdot\text{L}^{-1}$, $\text{MgSO}_4\cdot 7\text{H}_2\text{O}$ $0.5\text{ g}\cdot\text{L}^{-1}$, $\text{Ca}(\text{NO}_3)_2$ $0.01\text{ g}\cdot\text{L}^{-1}$, $\text{FeSO}_4\cdot 7\text{H}_2\text{O}$ $5.0\text{ g}\cdot\text{L}^{-1}$. The redox potential of solution was adjusted by addition of peroxide to setting value. The pH of solution was adjusted to 1.5 by adding H_2SO_4 .

2.4. Microbial Cultivation and Preparation

The microbial consortium used in the test was collected from an AMD site in Zijinshan mine, Fujian province, China, and the mixture of acidophiles was cultured in 9 K medium containing

5.0 g·L⁻¹ ferrous sulfate and 1% pyrite at pH 1.5 in an orbital incubator-shaker at 35 °C. After several passages, the diversity and stability of the microbial consortium were quite well. The microbes were harvested in the stationary phase. The microbial cells were collected by filtration on a 0.22 µm filter and washed with pH 1.5 sulfuric acid solution to remove iron from the culture medium. The cell number was determined by a Thoma counting chamber. The high-throughput sequencing method proved the microbial consortium has a similar composition and structure to real AMD microbial consortia.

2.5. Batch Experiments

All experiments were carried out in the same medium but under three different redox potential values. Two experiments were conducted at each redox potential value, in the presence and absence of microbes attached to pyrite. A microporous membrane installed in the filter plate can prevent microbial cells from attaching to pyrite. Both flasks were stirred by an overhead stirrer at a speed of 150 rpm and kept in a constant temperature bath. All leaching experiments were done at 35.0 ± 0.1 °C. The loading concentration was 10.0 g pyrite per liter. The concentration of total iron ions was 1.0 g·L⁻¹. The cell number in suspension was 10⁷ cells mL⁻¹. The solution containing microbes was replaced every 24 h. Total iron concentration was measured before and after leaching. The Fe concentration was measured using ICP-OES. After 7 days of leaching, pyrite residues were filtrated and washed with sulfate acid solution (pH = 1.5). After drying in a vacuum drying oven, the samples were stored in a refrigerator at -20 °C until testing.

2.6. Pyrite Surface Detection by SEM

After leaching experiments, the pyrite slabs were fixed with 3% glutaraldehyde in the same PBS solution (phosphate buffer at pH 7.2) overnight. The slabs were then dehydrated by immersing them in 50%, 75%, and 99% ethanol solutions for 30 min in sequence. Then, the slabs were air-dried in a fume hood for 2 h at room temperature. Finally, the slabs were gold-coated and observed by SEM (JSM-7800, JEOL, Tokyo, Japan) at 15 kV accelerating voltage.

2.7. X-Ray Photoelectron Spectroscopy (XPS) Analyses

The surface of residues under various solution environments was analyzed by an X-ray photoelectron spectrometer (ESCALAB 250Xi, Thermo Fisher Scientific, Waltham, MA, USA). The incident radiation was monochromatic Al K α X-rays (1486.7 eV) at 150W (15 kV, 15 mA). Base pressure in the analysis chamber was 2.31 × 10⁻¹⁰ mbar, and during sample analysis that was 2.31 × 10⁻⁸ mbar. Survey scans were taken to identify the elements present, and high-resolution scans were taken to determine the oxidation status and component of sulfur and iron. Data processing and fitting were carried out using Avantage v5.938 software package and the library of relative sensitivity factors (RSF). The spectra were charge referenced to adventitious C 1s peak at 284.8 eV and the Smart background subtraction method was used.

2.8. Quantification of Elemental Sulfur by HPLC

One gram of the pyrite residue was ultrasonically washed with alcohol three times. After centrifugation for 5 min at 8000 rpm, the supernatant was decanted to determine the concentration of elemental sulfur by high performance liquid chromatography (HPLC) (PD-M20A, Shimadzu, Japan) with a Hypersil-ODS-5µ column with pure methanol as eluent at a flow rate of 1 mL·min⁻¹ [6].

2.9. DNA Extraction and Microbial Consortium Analysis

To remove planktonic cells from the pyrite surface, residues were suspended in sulfuric acid solution (pH = 1.5) and washed gently. An indirect method was used to recover microbial cells attached to pyrite surface [30]. The DNA of the microbial consortium was extracted using a FastDNA Spin kit for soil according to the manufacturer's protocol. The F515 (5'-GTGYCAGCMGCCGCGGTAA) and

R806 (5'-GGACTACNVGGGTWCTAAT) primers were used to amplify the bacterial and archaeal 16S RNA genes V4 hyper variable region [31]. PCR reactions were performed in triplicate. Amplicons were separated with 2% agarose gels and extracted using the Axyprep DNA Gel Extraction Kit (Axygen Biosciences, Union City, CA, USA) according to the manufacturer's instructions. Purified amplicons were sequenced using the Illumina MiSeq platform according to the standard protocols [32]. Data were analyzed and quality-filtered using Quantitative Insights into Microbial Ecology (QIIME) [33]. Operational Units (OTU) were clustered at the sequence similarity level of 97% using UPARSE (version 7.1) and chimeric sequences were identified and discharged using UCHIME. The sequences were compared using BLAST against NCBI [34].

3. Results and Discussion

3.1. Morphological Characteristics of Residue Samples

The morphologies of pyrite residues were imaged by SEM. As Figure 3 showed, the higher the redox potential was, the severer the corrosion. Under each redox potential, the erosion of pyrite surface was similar irrespective of whether the attached microbes exist or not. The density of microbes was similar under three redox potentials. Furthermore, rod-shaped and spiral-shaped microorganisms could be seen under each redox potential. The pyrite surface was smooth with no obvious defects and fractures under 650 mV even with attached microbes. Pyrite with attached microbes showed no corrosion under 650 mV demonstrating that attached microbes cannot leach pyrite directly and EPS did not have a higher redox than the bulk solution. Small cracks and pits were observed on the surface under 750 mV. The width of the ditch was $0.29 \pm 0.03 \mu\text{m}$, similar to the width of cells, but the cracks were much longer. Much more serious erosion happened at 850 mV, the ditch was $0.92 \pm 0.05 \mu\text{m}$ wide, much wider than any attached microbes. Figure 3A also proved that no caves were directly formed on pyrite residue by contact leaching. The ditches were anisotropic, which showed pyrite leaching was easier at a specific crystal interplanar direction. The patterns of pitting and surface roughness were similar to those in previous reports [35–37]. The ditches formed in the presence of attached microbes were just a little wider than those in the absence of attached microbes, which indicating that attached microbes slightly accelerate pyrite leaching. According to the morphology information, the redox potential was essential for pyrite dissolution and microbes did not affect pyrite leaching fundamentally.

3.2. Kinetics under Different Redox Potentials and Microbial Conditions

The total iron concentration after leaching subtracting the iron added at the beginning of experiments gave a direct indication of pyrite leaching rates. The concentration was further converted into the dissolution percentage of pyrite and was plotted against time, as shown in Figure 4. Under any conditions, the dissolution rate was stable with time, implying a steady rate constant. The redox potential had a great impact on pyrite leaching regardless of whether or not microbes attached to pyrite. The attached acidophiles also improved pyrite leaching at 750 and 850 mV, which was backed up by t-tests analyses. The leaching rate in the absence of attached microbes, i.e., only with ferric iron working on the surface, can represent the contribution of "non-contact mechanism". The value calculated by subtracting the leaching rate with attached microorganisms from the rate without attached microorganisms under the same redox potential represented the contribution of sessile microbes or "contact mechanism". As the data were shown in Figure 4, the contribution of "non-contact mechanism" was $1.7 \pm 0.13\% \cdot \text{d}^{-1}$ in the means of dissolution percentage under 850 mV, more than 3 times bigger than that under 750 mV. The "contact mechanism" accelerated pyrite dissolution by about $0.30\% \cdot \text{d}^{-1}$ and $0.27\% \cdot \text{d}^{-1}$ at 750 and 850 mV, respectively. Under 650 mV, no pyrite oxidation was detected, which demonstrated that attached microbes cannot leach pyrite directly. These results suggest that "non-contact mechanism" plays a decisive role in pyrite dissolution under 750 and 850 mV and the attached microbes accelerate the oxidation of pyrite at a relatively low rate.

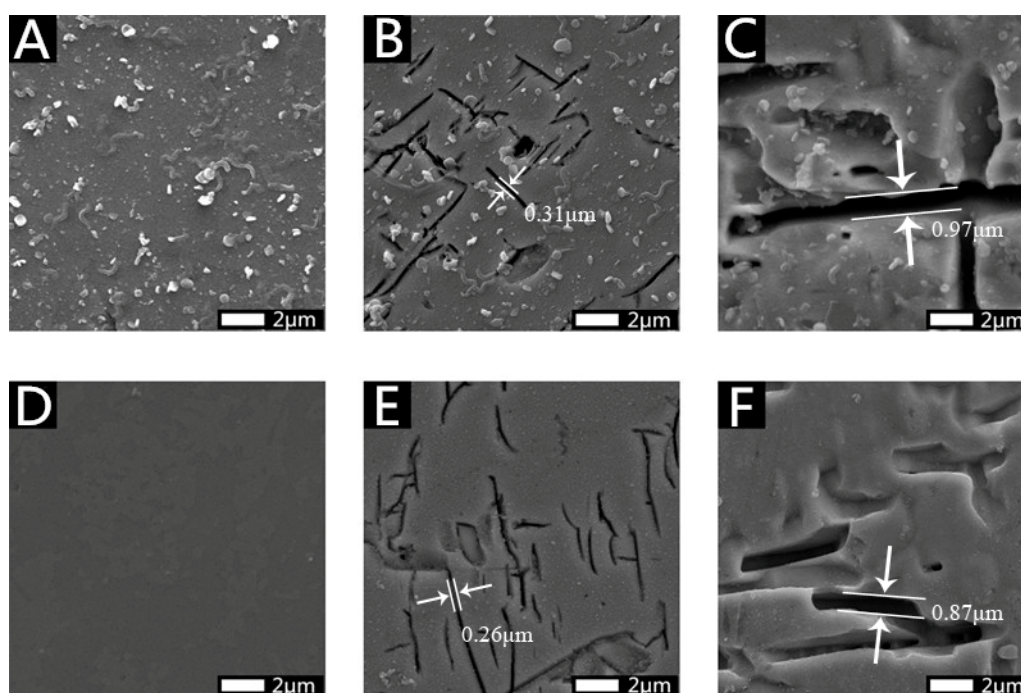


Figure 3. SEM photos of pyrite after leaching under different conditions: with attached microbes under (A) 650 mV, (B) 750 mV and, (C) 850 mV; without attached microbes under (D) 650 mV, (E) 750 mV and, (F) 850 mV.

When the redox potential of solution is similar to the rest potential of pyrite, the electron in pyrite does not tend to transfer between the solution and pyrite based on thermodynamics. The pyrite has a relatively high rest potential at around 660 mV [38], so pyrite cannot be oxidized at the redox potential of 650 mV. No pyrite leached out was observed in the presence of microbes and showed that cells cannot oxidize it directly. With increasing solution Eh, pyrite oxidation began, and the dissolution rate increased. At higher redox potential, for example, 750 and 850 mV, attached microbes helped pyrite leaching at a relatively slow rate. Initially, the cell-sized corrosion pit was considered as “contact leaching” [39,40], such an idea was questioned soon because chemical leaching also shows a cell-sized pit. The contribution of attached microbes to pyrite bioleaching was also studied by filtering the leaching microbes in solution [41]. Sessile acidophiles can also increase the redox potential and the pyrite can be oxidized by Fe^{3+} in solution, so the contribution of sessile microbes may be exaggerated. These studies have such a disadvantage that the data about redox potentials of solution were not recorded and discussed. Fowler et al. [42] found that pyrite had a slightly higher dissolution rate in the presence of microbes than in the absence of microbes under the same redox potential, due to the microbes’ increased the pH at the surface of the pyrite. However, they did not show more persuasive evidence. According to the physiological-biochemical characteristic of acidophiles, it is necessary to pump excess protons out from the acidophiles in order to maintain pH homeostasis [43]. It seems impossible that microbes can increase the pH at the pyrite surface. We speculate that attached cells act as a catalyst and accelerate the transformation of intermediate products. Because the experiments were conducted under a controlled redox potential, the iron oxidized by microbes would be reduced back to ferrous, and the ratio of ferric to ferrous is relatively constant. Therefore, it is the sulfur element that the attached microbes help to transform.

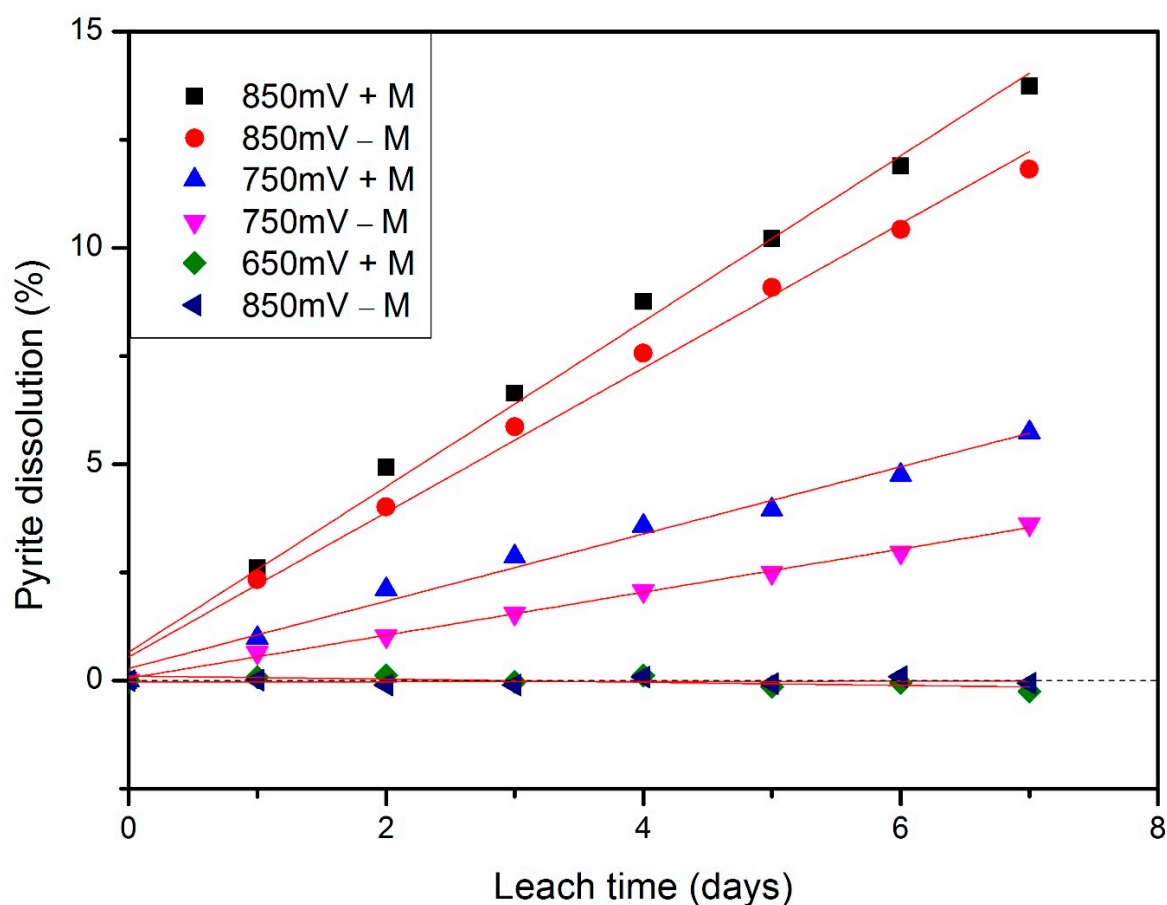


Figure 4. Effects of attached microbes on pyrite oxidation rate under different redox potentials. 850 mV + M: pyrite leaching with attached microbes under 850 mV; 850 mV - M: pyrite leaching without attached microbes under 850 mV; 750 mV + M: pyrite leaching with attached microbes under 750 mV; 750 mV - M: pyrite leaching without attached microbes under 750 mV; 650 mV + M: pyrite leaching with attached microbes under 650 mV; 650 mV - M: pyrite leaching without attached microbes under 650 mV.

3.3. XPS Characterization

XPS measurements were conducted to identify the surface products formed during leaching under different conditions. Figure 5 showed the S 2p spectra of pyrite residues. S 2p spectra were fitted using the 2p 1/2 and 2p 3/2 doublet with a fixed 1:2 intensity ratio. The doublet with S 2p3/2 located at 162.2–162.7 eV was attributed to disulfide S_2^{2-} from bulk pyrite [44]. The doublet at a lower binding energy range (161.5–162.0 eV) corresponded to the surface-most sulfur atom, S_2^{2-} [45]. The peak around 164.0 eV was attributed to polysulfide and elemental sulfur S_n^{2-}/S_8 [46,47]. An energy loss (EL) feature has been fitted at 164.5 eV. It was associated with S 3p to Fe 3d excitation [48,49]. The peak at around 168.5 eV was attributable to sulfate, which was originated from the sulfate ion in solution. The concentrations of every sulfur species were shown in Table S1. At 650 mV, the concentration of each sulfur species was similar between residue with attached microbes and that without attached microbes, a trace of elemental sulfur was detected, which may be formed during sample preparation [50]. At 750 mV, more elemental sulfur presented on the residue without attached microbes than that with attached microbes. At 850 mV, the difference of elemental sulfur content was more obvious between the two samples.

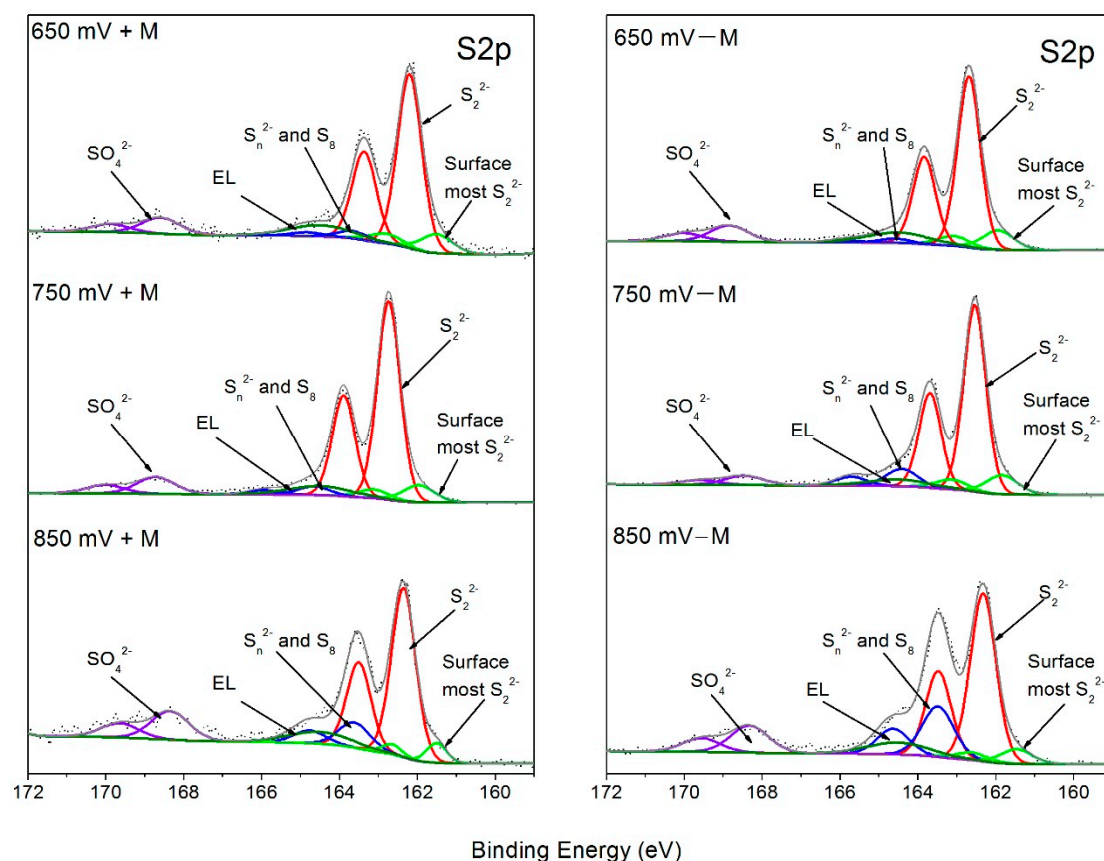


Figure 5. S 2p XPS spectra of pyrite surfaces under different conditions.

Figure 6 presented the Fe 2p 3/2 XPS spectra of each pyrite sample, and Table S2 showed the qualification of iron species based on the decoupling of the Fe 2p 3/2 XPS spectra. The main peak around 707.0 eV represented Fe(II) from the bulk pyrite. The two small peaks around 706.0 eV and 708.0 eV were the multiplet splitting peaks of Fe(II)-S [51]. The peak around 709.0 eV was attributed to Fe₃O₄/Fe₂O₃ and the higher energy peak around 710.5 eV represented the existence of FeOOH [52]. The Fe(III) species came from ferric in solution as well. At 650 mV, the percentage of Fe(III) species was higher on the sample without attached microbes than that with attached microbes. At 750 and 850 mV, the concentration of Fe(III) species did not show an obvious difference between the samples without and with attached microbes.

The XPS analysis showed that elemental sulfur was formed during pyrite oxidation. The peak of elemental sulfur displayed a much higher intensity on residue without attached microbes than that with attached microbes under 750 and 850 mV. This indicated that attached microbes metabolize the elemental sulfur which may lead to a higher leaching rate. Some researchers supposed that microbes accelerate pyrite leaching by limiting the formation of jarosite which causes pyrite passivation [25]. This idea was not supported by the XPS results, because the concentrations of Fe(III) species and sulfate did not show a difference between samples with attached microbes and without attached microbes under 750 and 850 mV.

3.4. Elemental Sulfur in Leaching Residue

As XPS results cannot show the precise amount of elemental sulfur, the HPLC tests were done, results were shown in Figure 7. At 650 mV, only an ignorable amount of elemental sulfur was detected regardless of whether there were attached microorganisms on pyrite or not. This agreed with no pyrite being leached at 650 mV. At 750 mV, more than 1100 µg elemental sulfur was produced without attached microorganisms from 1 g pyrite residue. At an even higher redox potential of 850 mV,

more than 2000 μg elemental sulfur per gram residue was produced from pyrite without attached microorganisms, which was almost two times higher than that under 750 mV. When sessile cells did not exist on the pyrite surface, the higher redox potential, the more elemental sulfur was produced as more pyrite leached. However, at 750 mV, almost all of the elemental sulfur was scavenged through biological metabolism, and most of elemental sulfur was oxidized by microbes under 850 mV as well. It is still true that higher redox potential leads to more elemental sulfur on the surface, but the elemental sulfur produced on the surface is alleviated by biological oxidation in the presence of attached microorganisms.

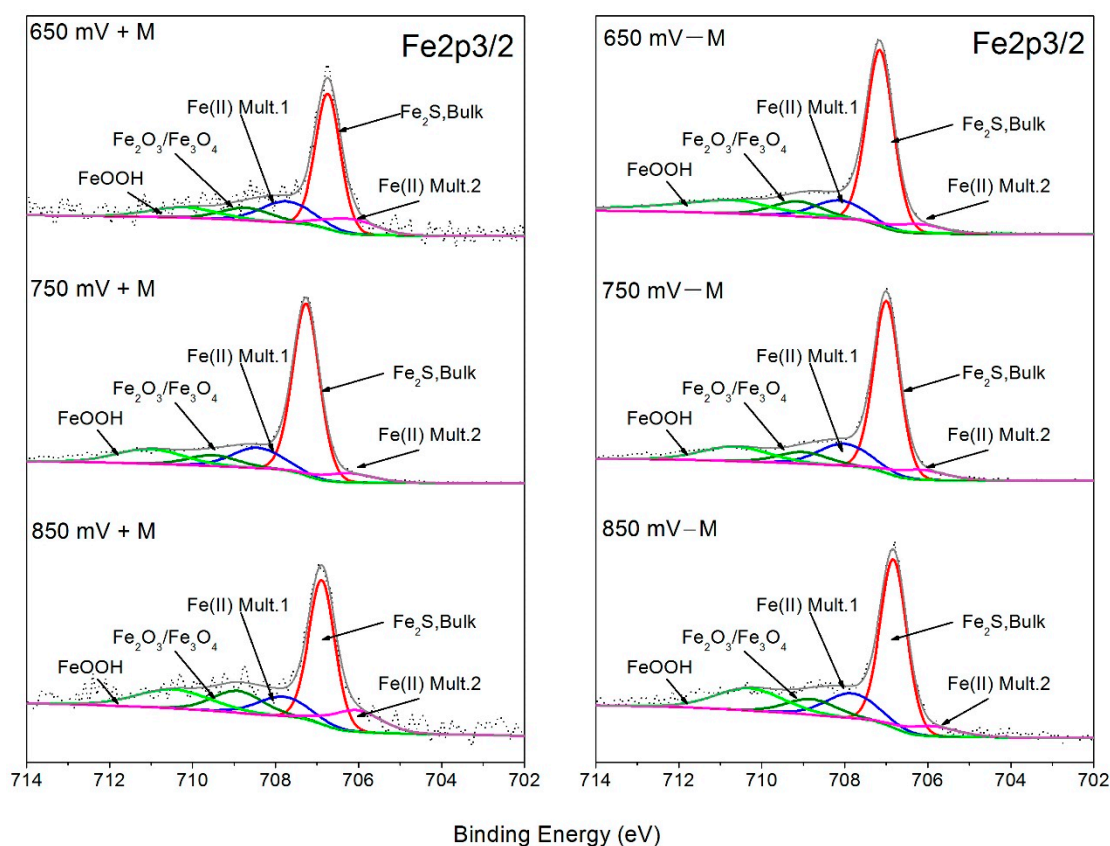


Figure 6. Fe 2p_{3/2} XPS spectra of pyrite surfaces under different conditions.

Some sulfide minerals such as chalcopyrite, chalcocite, and sphalerite yield quite a lot of elemental sulfur through the polysulfide mechanism in leaching. During the leaching of these minerals, it was found that a product layer covers a shrinking unreacted core that affects the leaching of those minerals obviously [53]. The elemental sulfur is formed via a quite complicated process during pyrite oxidation. Thiosulfate is the first free sulfur compound during pyrite leaching. A large number of thiosulfate ions are oxidized into tetrathionate on the pyrite surface, and the remaining small portion of thiosulfate is disproportionate to the elemental sulfur and sulfite ions [54]. In the presence of the related enzyme, tetrathionate is decomposed into disulfane-monosulfonic acid, which is very unstable and able to produce many other intermediate species [55]. In an acidic environment, polythionate degrades into elemental sulfur, thiosulfate, and sulfate [56]. When pyrite is chemically leached or bioleached by iron-oxidizing microbes without sulfur-oxidizing capacity, as much as 10% of pyritic sulfur moiety can turn into elemental sulfur [6,35]. When pyrite is leached by sulfur-oxidizers, only a small amount of elemental sulfur can be detected [37]. The solution was replaced every day which may lead to a loss of reduced elemental compounds in this research. The element sulfur forms in isolated patches rather than a continuous elemental sulfur layer at the surface [57]. In the solution, thiosulfate degrades into elemental sulfur, which is attached to the pyrite surface. Elemental sulfur is more hydrophobic

than pyrite. Thus, the later formed elemental sulfur is more likely to attach to the formerly formed elemental sulfur, leading to significantly increasing thickness and insignificantly increasing area of the isolated elemental sulfur patch. The production of an elemental sulfur layer can reduce the surface area of pyrite particles, leading to a slower pyrite leaching rate to a certain extent. The elemental sulfur forms in patches which can explain why elemental sulfur does not inhibit pyrite leaching significantly. It was also found during similar research that the accumulated elemental sulfur lowered the efficiency of pyrite oxidation [58,59]. The attached microbes can metabolize the elemental sulfur on the pyrite surface and thereby accelerate pyrite leaching.

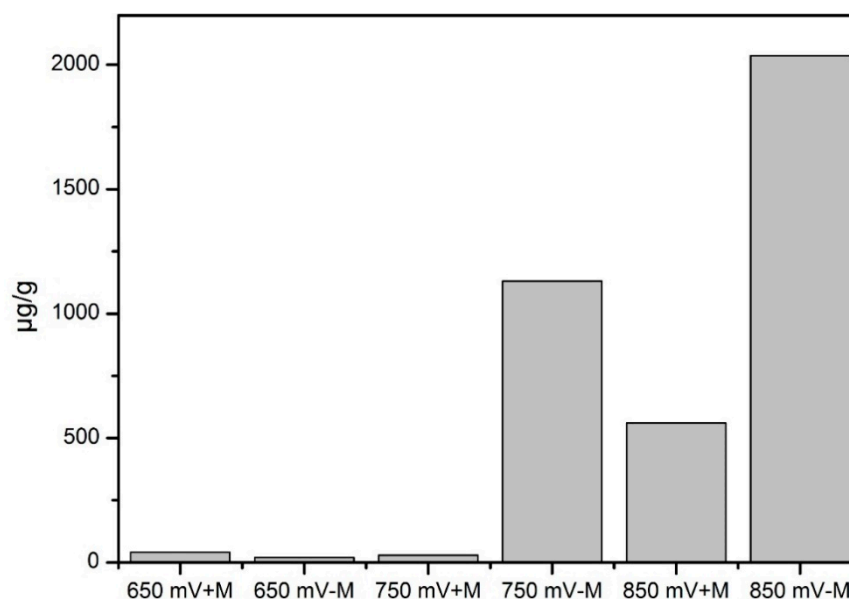


Figure 7. The concentration of elemental sulfur on pyrite under different redox potentials and microbial conditions.

3.5. Attached Microbial Community on Pyrite Residual

To know how attached microbes contribute to pyrite oxidation, it is necessary to know the species of attached microbes, especially the complex microbial consortium used in this research. The analysis of microbial consortium from simulated AMD obtained 73056 OTUs at 97% identity. After the removal of OTUs with <1% abundance, five species remained. The relative abundance of each species was shown in Figure 8.

In the planktonic sample, the most dominant species was *Leptospirillum ferriphilum* (61%) which only feeds on ferrous [60]. *Cuniculiplasma divulgatum* growing organoheterotrophically accounted for 20% [61]. *Acidithiobacillus caldus* accounting for 9% was capable of chemolithotrophic growth on reduced sulfur but incapable of growth with sulfide ores [62]. *Thermogymnomonas acidicola* feeding on ferrous accounted for 9% [63]. *Ferroplasma acidarmans* accounting for 1% can use organic matter and ferrous to grow [64]. The other species only accounted for about 1% in total and all of them can use ferrous and/or reduced sulfur. The composition agreed well with the former results of the microbial consortium in Zijinshan heap leaching [26]. The microorganisms detected here were also found in Richmond mine at Iron Mountain, California [23].

After the leaching experiments with attached microorganisms, a microbial consortium of attached microorganisms was analyzed. In all experiments at different redox potentials, the attached microbial consortium was mainly composed of two species: *A. caldus* and *L. ferriphilum*. The other species only accounted for less than 1%. At 650 mV, the relative abundance of *A. caldus* was 54% and *L. ferriphilum* accounted for 45%. The increased abundance of *A. caldus* showed that it had a higher tendency to attachment. At 750 mV, *A. caldus* accounted for 55%, and 44% accounted for *L. ferriphilum*. At 850 mV,

the attached microbes contained 90% *A. caldus* and only 10% *L. ferriphilum*. At all three redox potentials, *A. caldus* had much higher abundance than that in the added microbial consortium (8%). The elemental sulfur on pyrite surface may attract the sulfur-oxidizers. The effects of pure and mixed cultures of microbes on the dissolution of pyrite have been widely examined [15,25,35]. Pyrite can be oxidized by pure iron-oxidizers because the iron-oxidizer can produce ferric ion. Pure sulfur-oxidizer cannot dissolve pyrite, but a mixed culture consisting of iron-oxidizers and sulfur oxidizers can oxidize pyrite more rapidly, suggesting that sulfur-oxidizers can contribute to pyrite leaching indirectly. It is more likely that the ore surface is dominated by sulfur-oxidizers [65,66]. It was also found that *A. caldus* played an important role in arsenopyrite bioleaching. The proposed mechanism was that *A. caldus* moved the elemental sulfur that can cause an inhibitory of arsenopyrite leaching [67]. It is indubitable that a microbial consortium consisting of more sulfur-oxidizing microbes has stronger sulfur oxidation ability. The sulfur-oxidizing bacterium *A. caldus* became the most dominant species and the ferric-oxidizing bacterium *L. ferriphilum* decreased dramatically in sessile consortia under 750 and 850 mV, proving that the attached microbes enhance pyrite leaching by improving sulfur oxidation efficiency.

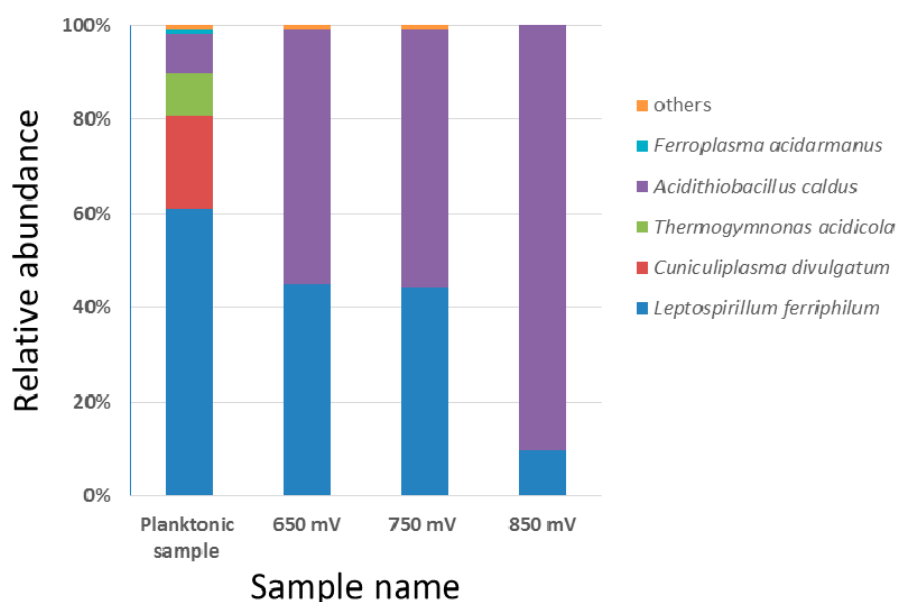


Figure 8. Relative abundance (%) of the dominant species in the planktonic sample and pyrite surface under different redox potentials. The species with a relative abundance of >1% were listed.

4. Conclusions

The morphology of pyrite after leaching revealed that sessile microbes accelerated pyrite leaching a little bit under 750 and 850 mV, as the corrosion was a little severer under the given redox potential. The attached microbes can accelerate pyrite leaching by eliminating the sulfur passivation even though they cannot oxidize pyrite directly. During pyrite leaching, some elemental sulfur was formed. Much more elemental sulfur was detected on pyrite samples in the absence of attached microbes than in the presence of attached microbes under 750 mV and 850 mV. Pyrite oxidation may be inhibited by elemental sulfur. The inhibition can be alleviated by the sulfur-oxidizing microbes on the surface of pyrite. The attached microbe consortia had a bigger percentage of sulfur-oxidizing microbes than the planktonic microbe consortia, and even sulfur-oxidizers became the dominant species, which further proved that the essence of “contact leaching” was sulfur oxidizers’ decrease in element sulfur passivation.

Supplementary Materials: The following are available online at <http://www.mdpi.com/2075-163X/10/10/856/s1>. Table S1: The percentage of S 2p species on the surfaces of residue under different conditions, Table S2: The percentage of Fe 2p_{3/2} species on the surfaces of residue under different conditions.

Author Contributions: Conceptualization, Y.J. and R.R.; investigation, B.D.; writing—original draft preparation, B.D.; writing—review and editing, Y.J. and R.R.; methodology, Q.T. and B.D.; data curation, H.S. All authors have read and agreed to the published version of the manuscript.

Funding: This work was supported by the National Natural Science Foundation of China (nos.51674231); Key Research Program of Chinese Academy of Sciences (no. ZDRW-ZS-2018-1); Innovation Academy for Green Manufacture, Chinese Academy of Sciences (IAGM-2019A08).

Acknowledgments: The support of State Key Laboratory of Biochemical Engineering is gratefully acknowledged.

Conflicts of Interest: The authors declare no conflict of interest.

References

1. Lundgren, D.; Silver, M. Ore Leaching by Bacteria. *Annu. Rev. Microbiol.* **1980**, *34*, 263–283. [[CrossRef](#)] [[PubMed](#)]
2. Suzuki, I. Microbial leaching of metals from sulfide minerals. *Biotechnol. Adv.* **2001**, *19*, 119–132. [[CrossRef](#)]
3. Vyas, S.; Ting, Y. Sequential biological process for molybdenum extraction from hydrodesulphurization spent catalyst. *Chemosphere* **2016**, *160*, 7–12. [[CrossRef](#)] [[PubMed](#)]
4. Vyas, S.; Ting, Y. Microbial leaching of heavy metals using *Escherichia coli* and evaluation of bioleaching mechanism. *Bioresour. Technol. Rep.* **2020**, *9*, 100368. [[CrossRef](#)]
5. Baker, B.; Banfield, J. Microbial communities in acid mine drainage. *FEMS Microbiol. Ecol.* **2003**, *44*, 139–152. [[CrossRef](#)]
6. Schippers, A.; Jozsa, P.; Sand, W. Sulfur chemistry in bacterial leaching of pyrite. *Appl. Environ. Microbiol.* **1996**, *62*, 3424–3431. [[CrossRef](#)]
7. Chandra, A.; Gerson, A. Redox potential (Eh) and anion effects of pyrite (FeS₂) leaching at pH 1. *Geochim. Cosmochim. Acta* **2011**, *75*, 6893–6911. [[CrossRef](#)]
8. Sun, H.; Chen, M.; Zou, L.; Shu, R.; Ruan, R. Study of the kinetics of pyrite oxidation under controlled redox potential. *Hydrometallurgy* **2015**, *155*, 13–19. [[CrossRef](#)]
9. Ma, J.; Tang, Y.; Yang, D.; Pei, P. Kinetics of advanced oxidative leaching of pyrite in a potassium peroxy-disulphate solution. *J. S. Afr. Inst. Min. Metall.* **2020**, *120*, 165–172. [[CrossRef](#)]
10. Bouffard, S.; Riverasquez, B.; Dixon, D. Leaching kinetics and stoichiometry of pyrite oxidation from a pyrite–marcasite concentrate in acid ferric sulfate media. *Hydrometallurgy* **2006**, *84*, 225–238. [[CrossRef](#)]
11. Qian, G.; Fan, R.; Short, M.; Schumann, R.; Li, J.; Smart, R.; Gerson, A. The Effects of Galvanic Interactions with Pyrite on the Generation of Acid and Metalliferous Drainage. *Environ. Sci. Technol.* **2018**, *52*, 5349–5357. [[PubMed](#)]
12. Liu, C.; Jia, Y.; Sun, H.; Tan, Q.; Niu, X.; Leng, X.; Ruan, R. Limited role of sessile acidophiles in pyrite oxidation below redox potential of 650 mV. *Sci. Rep.* **2017**, *7*, 5032–5040. [[PubMed](#)]
13. Vera, M.; Schippers, A.; Sand, W. Progress in bioleaching: Fundamentals and mechanisms of bacterial metal sulfide oxidation—Part A. *Appl. Microbiol. Biotechnol.* **2013**, *97*, 7529–7541. [[PubMed](#)]
14. Rodriguez, Y.; Ballester, A.; Blazquez, M.; González, F.; Munoz, J. New information on the pyrite bioleaching mechanism at low and high temperature. *Hydrometallurgy* **2003**, *71*, 37–46.
15. Sand, W.; Gehrke, T.; Jozsa, P.G.; Schippers, A. (Bio) chemistry of bacterial leaching—Direct vs. indirect bioleaching. *Hydrometallurgy* **2001**, *59*, 159–175. [[CrossRef](#)]
16. Silverman, M.; Ehrlich, H. Microbial formation and degradation of minerals. *Adv. Appl. Microbiol.* **1964**, *6*, 153–206.
17. Tributsch, H. Direct versus indirect bioleaching. *Hydrometallurgy* **2001**, *59*, 177–185. [[CrossRef](#)]
18. Rohwerder, T.; Gehrke, T.; Kinzler, K.; Sand, W. Bioleaching review part A. *Appl. Microbiol. Biotechnol.* **2003**, *63*, 239–248. [[CrossRef](#)]
19. McKibben, M.; Barnes, H. Oxidation of pyrite in low temperature acidic solutions: Rate laws and surface textures. *Geochim. Cosmochim. Acta* **1986**, *50*, 1509–1520. [[CrossRef](#)]

20. Govender, E.; Kotsiopoulos, A.; Bryan, C.; Harrison, S. Modelling microbial transport in simulated low-grade heap bioleaching systems: The hydrodynamic dispersion model. *Chem. Eng. Sci.* **2017**, *172*, 545–558. [[CrossRef](#)]
21. Liu, J.; Li, Q.; Sand, W.; Zhang, R. Influence of *Sulfobacillus thermosulfidooxidans* on initial attachment and pyrite leaching by thermoacidophilic archaeon *Acidianus* sp. DSM 29099. *Minerals* **2016**, *6*, 76. [[CrossRef](#)]
22. Li, Q.; Zhu, J.; Li, S.; Zhang, R.; Xiao, T.; Sand, W. Interactions between cells of *Sulfobacillus thermosulfidooxidans* and *Leptospirillum ferriphilum* during pyrite bioleaching. *Front. Microbiol.* **2020**, *11*, 44. [[CrossRef](#)] [[PubMed](#)]
23. Bond, P.; Smriga, S.; Banfield, J. Phylogeny of microorganisms populating a thick, subaerial, predominantly lithotrophic biofilm at an extreme acid mine drainage site. *Appl. Environ. Microbiol.* **2000**, *66*, 3842–3849. [[CrossRef](#)]
24. Chen, L.; Hu, M.; Huang, L.; Hua, Z.; Kuang, J.; Li, S.; Shu, W. Comparative metagenomic and metatranscriptomic analyses of microbial communities in acid mine drainage. *ISME J.* **2015**, *9*, 1579–1592. [[CrossRef](#)]
25. Okibe, N.; Johnson, D. Biooxidation of pyrite by defined mixed cultures of moderately thermophilic acidophiles in pH-controlled bioreactors: Significance of microbial interactions. *Biotechnol. Bioeng.* **2004**, *87*, 574–583. [[CrossRef](#)] [[PubMed](#)]
26. Xiao, Y.; Liu, X.; Ma, L.; Liang, Y.; Niu, J.; Gu, Y.; Zhang, X.; Hao, X.; Dong, W.; She, S. Microbial communities from different subsystems in biological heap leaching system play different roles in iron and sulfur metabolisms. *Appl. Microbiol. Biotechnol.* **2016**, *100*, 6871–6880. [[CrossRef](#)]
27. Xian, H.; Zhu, J.; Tan, W.; Tang, H.; Liu, P.; Zhu, R.; Liang, X.; Wei, J.; He, H.; Henry, T. The mechanism of defect induced hydroxylation on pyrite surfaces and implications for hydroxyl radical generation in prebiotic chemistry. *Geochim. Cosmochim. Acta* **2018**, *244*, 263–272. [[CrossRef](#)]
28. Caldeira, C.; Ciminelli, V.; Osseasare, K. The role of carbonate ions in pyrite oxidation in aqueous systems. *Geochim. Cosmochim. Acta* **2010**, *74*, 1777–1789. [[CrossRef](#)]
29. Silverman, M. Studies on the chemoautotrophic iron bacterium *ferrobacillus ferrooxidans*. *J. Bacteriol.* **1959**, *77*, 642–647. [[CrossRef](#)]
30. Tan, G.; Shu, W.; Hallberg, K.; Li, F.; Lan, C.; Zhou, W.; Huang, L. Culturable and molecular phylogenetic diversity of microorganisms in an open-dumped, extremely acidic Pb/Zn mine tailings. *Extremophiles* **2008**, *12*, 657. [[CrossRef](#)]
31. Bates, S.; Berglyons, D.; Caporaso, J.; Walters, W.; Knight, R.; Fierer, N. Examining the global distribution of dominant archaeal populations in soil. *ISME J.* **2011**, *5*, 908–917. [[CrossRef](#)] [[PubMed](#)]
32. Xiao, Y.; Xu, Y.; Dong, W.; Liang, Y.; Fan, F.; Zhang, X.; Zhang, X.; Niu, J.; Ma, L.; She, S. The complicated substrates enhance the microbial diversity and zinc leaching efficiency in sphalerite bioleaching system. *Appl. Microbiol. Biotechnol.* **2015**, *99*, 10311–10322. [[CrossRef](#)] [[PubMed](#)]
33. Caporaso, J.; Kuczynski, J.; Stombaugh, J.; Bittinger, K.; Bushman, F.; Costello, E.; Fierer, N.; Pena, A.; Goodrich, J.; Gordon, J. QIIME allows analysis of high-throughput community sequencing data. *Nat. Methods* **2010**, *7*, 335–336. [[CrossRef](#)] [[PubMed](#)]
34. Altschul, S.; Gish, W.; Miller, W.; Myers, E.; Lipman, D. Basic Local Alignment Search Tool. *J. Mol. Biol.* **1990**, *215*, 403–410. [[CrossRef](#)]
35. McGuire, M.; Edwards, K.; Banfield, J.; Hamers, R. Kinetics, surface chemistry, and structural evolution of microbially mediated sulfide mineral dissolution. *Geochim. Cosmochim. Acta* **2001**, *65*, 1243–1258. [[CrossRef](#)]
36. Yang, Y.; Tan, S.; Glenn, A.; Harmer, S.; Bhargava, S.; Chen, M. A direct observation of bacterial coverage and biofilm formation by *Acidithiobacillus ferrooxidans* on chalcopyrite and pyrite surfaces. *Biofouling* **2015**, *31*, 575–586. [[CrossRef](#)]
37. Tu, Z.; Guo, C.; Zhang, T.; Lu, G.; Wan, J.; Liao, C.; Dang, Z. Investigation of intermediate sulfur species during pyrite oxidation in the presence and absence of *Acidithiobacillus ferrooxidans*. *Hydrometallurgy* **2017**, *167*, 58–65. [[CrossRef](#)]
38. Li, Y.; Kawashima, N.; Li, J.; Chandra, A.; Gerson, A. A review of the structure, and fundamental mechanisms and kinetics of the leaching of chalcopyrite. *Adv. Colloid Interface Sci.* **2013**, *197*, 1–32. [[CrossRef](#)]
39. Gehrke, T.; Telegdi, J.; Thierry, D.; Sand, W. Importance of extracellular polymeric substances from *Thiobacillus ferrooxidans* for bioleaching. *Appl. Environ. Microbiol.* **1998**, *64*, 2743–2747. [[CrossRef](#)]

40. Becker, T.; Gorham, N.; Shiers, D.; Watling, H. In situ imaging of *Sulfobacillus thermosulfidooxidans* on pyrite under conditions of variable pH using tapping mode atomic force microscopy. *Process Biochem.* **2011**, *46*, 966–976. [[CrossRef](#)]
41. Bellenberg, S.; Barthen, R.; Boretska, M.; Zhang, R.; Sand, W.; Vera, M. Manipulation of pyrite colonization and leaching by iron-oxidizing *Acidithiobacillus* species. *Process Biochem.* **2015**, *99*, 1435–1449. [[CrossRef](#)] [[PubMed](#)]
42. Fowler, T.; Holmes, P.; Crundwell, F. Mechanism of Pyrite Dissolution in the Presence of *Thiobacillus ferrooxidans*. *Appl. Environ. Microbiol.* **1999**, *65*, 2987–2993. [[CrossRef](#)] [[PubMed](#)]
43. Michels, M.; Bakker, E.P. Generation of a large, protonophore-sensitive proton motive force and pH difference in the acidophilic bacteria *Thermoplasma acidophilum* and *Bacillus acidocaldarius*. *J. Bacteriol.* **1985**, *161*, 231–237. [[CrossRef](#)] [[PubMed](#)]
44. Chen, X.; Peng, Y.; Bradshaw, D. Effect of regrinding conditions on pyrite flotation in the presence of copper ions. *Int. J. Miner. Process.* **2013**, *125*, 129–136. [[CrossRef](#)]
45. Nesbitt, H.; Bancroft, G.; Pratt, A.; Scaini, M. Sulfur and iron surface states on fractured pyrite surfaces. *Am. Mineral.* **1998**, *83*, 1067–1076. [[CrossRef](#)]
46. Huai, Y.; Plackowski, C.; Peng, Y. The surface properties of pyrite coupled with gold in the presence of oxygen. *Miner. Eng.* **2017**, *111*, 131–139. [[CrossRef](#)]
47. Huai, Y.; Plackowski, C.; Peng, Y. The effect of gold coupling on the surface properties of pyrite in the presence of ferric ions. *Appl. Surf. Sci.* **2019**, *488*, 277–283. [[CrossRef](#)]
48. Acres, R.; Harmer, S.; Beattie, D. Synchrotron XPS studies of solution exposed chalcopyrite, bornite, and heterogeneous chalcopyrite with bornite. *Int. J. Miner. Process.* **2010**, *94*, 43–51. [[CrossRef](#)]
49. Chen, X.; Peng, Y. The effect of regrind mills on the separation of chalcopyrite from pyrite in cleaner flotation. *Miner. Eng.* **2015**, *83*, 33–43. [[CrossRef](#)]
50. Schaufuss, A.; Nesbitt, H.; Kartio, I.; Laajalehto, K.; Bancroft, G.; Szargan, R. Reactivity of surface chemical states on fractured pyrite. *Surf. Sci.* **1998**, *411*, 321–328. [[CrossRef](#)]
51. Ejtemaei, M.; Nguyen, A. Characterisation of sphalerite and pyrite surfaces activated by copper sulphate. *Miner. Eng.* **2017**, *100*, 223–232.
52. Cai, Y.; Pan, Y.; Xue, J.; Sun, Q.; Su, G.; Li, X. Comparative XPS study between experimentally and naturally weathered pyrites. *Appl. Surf. Sci.* **2009**, *255*, 8750–8760.
53. Niu, X.; Ruan, R.; Tan, Q.; Jia, Y.; Sun, H. Study on the second stage of chalcocite leaching in column with redox potential control and its implications. *Hydrometallurgy* **2015**, *155*, 141–152.
54. Xu, Y.; Schoonen, M.A. The stability of thiosulfate in the presence of pyrite in low-temperature aqueous solutions. *Geochim. Cosmochim. Acta* **1995**, *59*, 4605–4622.
55. Steudel, R.; Holdt, G.; Göbel, T.; Hazeu, W. Chromatographic separation of higher polythionates SnO ($n = 3 \dots 22$) and their detection in cultures of *Thiobacillus ferrooxidans*; molecular composition of bacterial Sulfur secretions. *Angew. Chem. Int. Edit.* **1987**, *26*, 151–153.
56. De Jong, G.; Hazeu, W.; Bos, P.; Kuenen, J. Polythionate degradation by tetrathionate hydrolase of *Thiobacillus ferrooxidans*. *Microbiology* **1997**, *143*, 499–504.
57. Mcguire, M.; Jallad, K.; Ben-Amotz, D.; Hamers, R. Chemical mapping of elemental sulfur on pyrite and arsenopyrite surfaces using near-infrared Raman imaging microscopy. *Appl. Surf. Sci.* **2001**, *178*, 105–115.
58. Tu, Z.; Wan, J.; Guo, C.; Fan, C.; Zhang, T.; Lu, G.; Reinfelder, J.; Dang, Z. Electrochemical oxidation of pyrite in pH 2 electrolyte. *Electrochim. Acta* **2017**, *239*, 25–35.
59. Schippers, A.; Rohwerder, T.; Sand, W. Intermediary sulfur compounds in pyrite oxidation: Implications for bioleaching and biodepyritization of coal. *Appl. Microbiol. Biotechnol.* **1999**, *52*, 104–110.
60. Panyushkina, A.; Tsaplina, I.; Kondrat'eva, T.; Belyi, A.; Bulaev, A. Physiological and Morphological Characteristics of Acidophilic Bacteria *Leptospirillum ferriphilum* and *Acidithiobacillus thiooxidans*, Members of a Chemolithotrophic Microbial Consortium. *Microbiology* **2018**, *87*, 326–338.
61. Golyshina, O.V.; Lünsdorf, H.; Kublanov, I.V.; Goldenstein, N.I.; Hinrichs, K.-U.; Golyshin, P.N. The novel extremely acidophilic, cell-wall-deficient archaeon *Cuniculiplasma divulgatum* gen. nov., sp. nov. represents a new family, *Cuniculiplasmataceae* fam. nov., of the order *Thermoplasmatales*. *Int. J. Syst. Evol. Microbiol.* **2016**, *66*, 332. [[CrossRef](#)] [[PubMed](#)]
62. Hallberg, K.; Lindstrom, E. Characterization of *Thiobacillus caldus* sp. nov., a moderately thermophilic acidophile. *Microbiology* **1994**, *140*, 3451–3456. [[PubMed](#)]

63. Yelton, A.; Thomas, B.; Simmons, S.; Wilmes, P.; Zemla, A.; Thelen, M.; Justice, N.; Banfield, J. A semi-quantitative, synteny-based method to improve functional predictions for hypothetical and poorly annotated bacterial and archaeal genes. *PLoS Comput. Biol.* **2011**, *7*, 10. [[CrossRef](#)] [[PubMed](#)]
64. Golyshina, O.; Pivovarova, T.; Karavaiko, G.; Kondratéva, T.; Moore, E.; Abraham, W.; Lünsdorf, H.; Timmis, K.; Yakimov, M.; Golyshin, P. *Ferroplasma acidiphilum* gen. nov., sp. nov., an acidophilic, autotrophic, ferrous-iron-oxidizing, cell-wall-lacking, mesophilic member of the Ferroplasmaceae fam. nov., comprising a distinct lineage of the Archaea. *Int. J. Syst. Evol. Microbiol.* **2000**, *50*, 997–1006. [[CrossRef](#)]
65. Mutch, L.; Watling, H.; Watkin, E. Microbial population dynamics of inoculated low-grade chalcopyrite bioleaching columns. *Hydrometallurgy* **2010**, *104*, 391–398. [[CrossRef](#)]
66. Ma, L.; Wang, X.; Feng, X.; Liang, Y.; Xiao, Y.; Hao, X.; Yin, H.; Liu, H.; Liu, X. Co-culture microorganisms with different initial proportions reveal the mechanism of chalcopyrite bioleaching coupling with microbial community succession. *Bioresour. Technol.* **2017**, *223*, 121–130.
67. Dopson, M.; Lindström, E. Potential role of *Thiobacillus caldus* in arsenopyrite bioleaching. *Appl. Environ. Microbiol.* **1999**, *65*, 36–40. [[CrossRef](#)]



© 2020 by the authors. Licensee MDPI, Basel, Switzerland. This article is an open access article distributed under the terms and conditions of the Creative Commons Attribution (CC BY) license (<http://creativecommons.org/licenses/by/4.0/>).